Available online at www.sciencedirect.com
SCIENCE DIRECT®
Polymer 45 (2004) 3001–3016
polymer
www.elsevier.com/locate/polymer

Viscoelastic properties and morphology of sulfonated poly(styrene-*b*-ethylene/butylene-*b*-styrene) block copolymers (sBCP), and sBCP/[silicate] nanostructured materials

Kenneth A. Mauritz[a,*], Richard I. Blackwell[a], Frederick L. Beyer[b]

[a]*Department of Polymer Science, The University of Southern Mississippi, Southern Station Box 10076, Hattiesburg, MS 39406-0076, USA*
[b]*Polymers Research Branch, U.S. Army Research Laboratory, Aberdeen Proving Ground, Aberdeen, MD 21005-5069, USA*

Received 14 July 2003; received in revised form 15 December 2003; accepted 17 December 2003

Abstract

Self-assembled organic/inorganic hybrid materials were created via domain targeted sol–gel reactions of tetraethylorthosilicate in solution with sulfonated poly(styrene-*b*-[ethylene-*co*-butylene]-*b*-styrene) (sSEBS) copolymers. Dynamic mechanical analyses (DMA) of these hybrid materials suggest that the silicate component preferentially incorporates within the sulfonated polystyrene (PS) domains. An irreversible order–order transition (OOT) for unmodified SEBS, sSEBS, and the organic/inorganic hybrids was identified using DMA in shear mode. The OOT temperature increases with sulfonation as well as by adding a silicate phase by the sol–gel process. The DMA results imply a morphological shift with sulfonation, and reflect modified interactions within and between phases. Atomic force microscopy (AFM) indicated a shift from hexagonally packed cylinders in unmodified SEBS to a lamellar morphology in the sulfonated materials, but silicate incorporation did not affect the morphology or domain dimensions. The latter result is evidence for sol–gel polymerization templating in a self-assembly process. The phase-separated morphology is stable up to the degradation temperature of the polymer and thermogravimetric analysis revealed that the degradation temperature is unaffected by silicate incorporation. Small angle X-ray scattering data are in harmony with the structures revealed by AFM in terms of degree of order and scale of features. These results are largely rationalized in terms of chain mobility restrictions due to hydrogen-bonding interactions between different sulfonated PS blocks, an increase in the PS-ethylene/butylene block mixing parameter, increased interfacial surface tension and chain restrictions posed by inserted silicate nanostructures in the case of the hybrid materials.

Keywords: Block copolymer ionomer; Sol–gel reaction template; Self-assembled nanocomposite

1. Introduction

The phase-separated morphologies of functionalized polystyrene (PS)—containing block copolymers (BCP) can act as 3-dimensional templates for sol–gel polymerizations of inorganic alkoxides. 'Template' refers to the growth of inorganic oxide or organically modified silicate structures within a specific nanostructured BCP phase based on the miscibility of hydrolyzed alkoxide monomers within this targeted phase. Early investigations involved sol–gel reactions for tetraethylorthosilicate (TEOS) in pre-cast films of [sulfonated PS (sPS)]-*co*-polyisobutylene (PIB)-*co*-[sulfonated PS (sPS)] that were swollen in a PS domain-selective solvent [1,2]. The increased polarity of the PS blocks caused by sulfonation encourages the selective diffusion of polar hydrolyzed TEOS monomers to this phase where sol–gel reactions culminate in highly condensed silicate quasi-networks that reside exclusively within/around the PS phase, as depicted in Fig. 1. Generally, factors that influence sol–gel reactions include the H_2O:Si-OR mole ratio, pH, temperature, reaction time, and drying conditions [3]. An acid or base catalyst can be used, although in the work presented here, no catalyst was used since the attached sulfonic acid groups automatically serve in this capacity.

Dynamic mechanical analysis (DMA) and transmission and atomic force microscopy (AFM) have provided evidence that supports the template hypothesis in the sPS-PIB-sPS—based systems.

* Corresponding author. Tel.: +1-601-266-5595; fax: +1-601-266-5635.
E-mail address: kenneth.mauritz@usm.edu (K.A. Mauritz).

0032-3861/$ - see front matter © 2004 Elsevier Ltd. All rights reserved.
doi:10.1016/j.polymer.2003.12.078

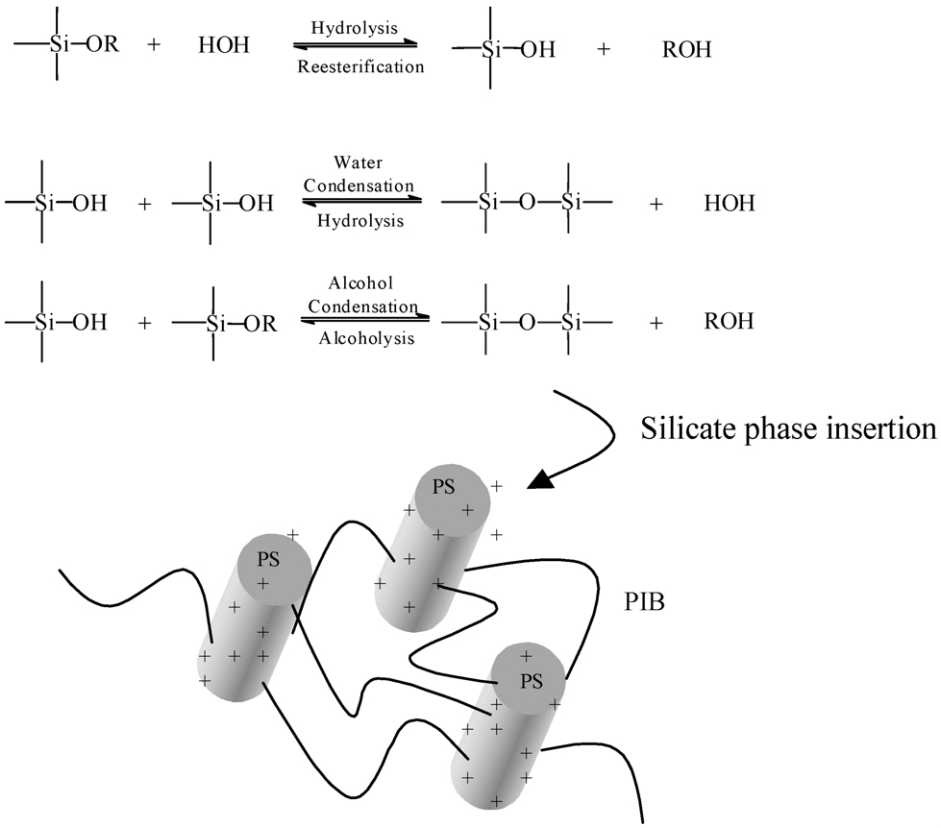

Fig. 1. General sol–gel reaction scheme and illustration of sPS domain-targeted silicate structure insertion.

The in situ sol–gel process that utilizes pre-formed film templates involves the variables of alkoxide monomer permeation time, and film thickness and size. However, these variables usually affect a non-uniform distribution of silicate across the film. Inorganic oxide concentration gradients may in fact be desirable in some cases, e.g., membranes with required asymmetry, but uniform concentrations might be required for others. Also, there can be a problem in the form of undesired silica precipitation on film surfaces rather in the interior. The process described below alleviates these problems.

More recently, these nanocomposites have been formulated in such a way that all of the molecular building blocks (BCP + sol–gel monomer + solvent + water) are present in co-miscible precursor solutions and the resultant dried materials are self-assembled. In addition to achieving successful self-assembly using the experimental sPS-PIB-sPS materials, the principle has been demonstrated to be operative for commercial poly(styrene-*co*-ethylene/butylene (EB)-*co*-styrene) tri-BCPs (commercial Kraton®), whose outer blocks are sulfonated [4–6]. Apparently, the kinetics and microstructural evolution of the polymer component during film formation do not interfere with the kinetics of the sol–gel reaction while hydrolyzed silicate monomers preferentially migrate to the sPS domains. The hybrid materials discussed here were fabricated by this latter, less-restrictive method.

The geometry of a minor PS phase in these Kraton® tri-BCPs evolves in the usual order, namely spheres → cylinders → lamellae with increasing PS volume fraction, f_{PS} [7,8]. Microphase separation is thermodynamically driven by an unfavorable interaction parameter, χ_{S-EB}, for the S and EB blocks. BCP morphology is also influenced by rate of cooling from the liquid state, annealing and solvent type in the case of solvent-cast films and the morphology near the surface may not be the same as that within the bulk.

For blocks A and B in the more often studied di-block copolymers, phase behavior is determined, in addition to f_{AB}, by $\chi_{AB}N$, where χ_{AB} is the A–B interaction parameter and N is the degree of polymerization in a monodisperse sample, as discussed by Leibler [9]. For symmetric di-BCPs, the condition $\chi_{AB}N \gg 10.5$ defines the strong segregation limit (SSL) where nearly pure A and B microdomains exist and inter-phase dimensions are small relative to domain spacings. The weak segregation limit (WSL) is defined by $\chi_{AB}N \leq 10.5$. Because χ_{AB} is inversely proportional to temperature, the BCPs exhibit a phenomenon analogous to an upper critical solution temperature (UCST) in polymer blends [10]. BCPs in the SSL and WSL regimes have been extensively studied by several investigators [11].

Above a critical temperature, χ_{AB} is sufficiently reduced to allow for statistical mixing of the two dissimilar blocks and there is an order–disorder transition (ODT). Leibler constructed phase diagrams that predict the ODT at various

f_{AB}. In the WSL, the phase diagrams also predict an order–order transition (OOT) that corresponds to a mesophase shift, for example, from hexagonal packed cylinders (HPC) to body centered cubic spheres (BCC) at temperatures approaching the ODT. The ODT and OOT for several BCPs have been evaluated using a variety of methods, including rheological measurements [12–19], differential scanning calorimetry [20,21], small angle X-ray scattering analysis (SAXS) [10,12,22–27], small angle neutron scattering analysis [8,28], microscopy [8,18,19] and dynamic light scattering [29,30].

While the systems reported here are more complex, the concepts described above are applicable in a general sense and will be used to guide data interpretation. The first added complexity is sulfonation of the PS blocks, which introduces strong electrostatic interactions. AFM [31] and SAXS [32] studies of morphology showed that sulfonation of PS-PIB-PS materials and subsequent silicate inclusion do not affect the cylindrical morphology or inter-domain spacings. Weiss et al. reported that sulfonation did influence the morphology of SEBS, poly(styrene-*b*-ethylene/propylene) (SEP) and poly(styrene-*b*-ethylene/propylene-*b*-styrene) (SEPS) BCPs. Depending on counterion type, sulfonation can hinder the formation of a well ordered morphology. They observed a shift from HPC to lamellar (L) upon sulfonation of the SEP as well as an increase in the inter-domain spacing, although this transformation did not occur with SEPS. HPC was maintained up to 8.7% sulfonation, regardless of counterion [33]. For the SEBS samples, 5% sulfonation with a Zn^{2+} counterion also showed a shift from HPC to L. The Na^{+} counterion form did not exhibit long-range order, which was attributed to the stronger ionic interactions that hindered chain mobility [34]. SAXS data for a 12% acid form SEBS also indicated a shift from HPC to L at 175 °C [35]. Morphological shifts affected by sulfonation and ion-neutralization that are similar to those reported by Weiss et al. are reported here.

Other researchers have performed sol–gel reactions in similar BCPs. Chen et al. created (four-arm star styrene-butadiene block copolymer elastomer)/silicate hybrid materials via an in situ sol–gel process for TEOS and concluded that the silicate network resided within the PS domains [36]. Huang et al. covalently attached a TiO_2-SiO_2 phase to amine-functionalized PS domains of an SEBS polymer through a glycidyloxypropyl trimethoxysilane linking agent [37]. Ikeda et al. also carried out sol–gel reactions of TEOS within cross-linked styrene-butadiene block copolymers, though no templating effect was observed [38].

The work reported here deals with an assessment of the influence of sulfonation, and then the effect of the inorganic sol–gel modification of the sulfonated block copolymers, on what appears to be an order–order transition of SEBS. This transition was investigated by monitoring the dynamic mechanical shear modulus, G', vs. temperature. Inferences were made regarding the location of the silicate component from the behavior of the sPS and EB block T_g values. The morphologies of these materials were established using AFM and SAXS and related to the viscoelastic results.

2. Experimental

2.1. Materials

All reagents were used without further purification. TEOS (98%), 1,2-dichloroethane (DCE) (99.8%), toluene, 1-hexanol (98%), acetic anhydride (ACS grade), and sulfuric acid (ACS grade) were obtained from Fisher Co. The SEBS copolymer, Kraton® G1652, was obtained from Kraton® LLC. The SEBS materials had $M_n \sim 70{,}000$ g mol^{-1} as determined by GPC, and a PS block content of ~30 mol% as determined from ^{1}H NMR. For this composition, the morphology is known to consist of hexagonally packed cylinders of PS blocks with good long ranged order.

Films of the parent SEBS materials were cast from a toluene solution into PTFE coated pans and allowed to dry at 60 °C for 5d followed by annealing under vacuum at 120 °C for 3d.

2.2. BCP sulfonation

Sulfonation of SEBS was carried out according to the procedure developed by Weiss et al. [39]. In summary, SEBS was dissolved in DCE at 50 °C. The sulfonating agent, acetyl sulfate, was generated by addition of sulfuric acid to a solution of acetic anhydride in DCE. The amount of acetyl sulfate required for the desired level of sulfonation was added to the polymer solution. The reaction proceeded for 2 h and the polymer was recovered by steam stripping. The sulfonated SEBS (sSEBS) was dried at room temperature under vacuum until constant mass was achieved.

Mole percent sulfonation was determined by titration. sSEBS samples were dissolved in a toluene/hexanol mixture. This solution was heated to 80 °C and titrated against 0.02 M tetrabutylammonium hydroxide (TBAH) in methanol to a phenolphthalein endpoint. The TBAH solution was standardized against solutions of *p*-toluene sulfonic acid. For all of the results presented herein, the sSEBS remained in the acid form, denoted in terms of percent sulfonation by x% H^+.

In film preparation, the same solvent was used for sSEBS samples as for SEBS. The casting and annealing conditions were the same for all the samples in this work.

2.3. Sol–gel reaction

The desired level of silicate incorporation in all samples reported here was 10 wt%, unless otherwise noted. sSEBS samples were dissolved in a toluene/hexanol mixture. The necessary amount of TEOS and deionized water were added

to the solution and stirred for 4 h. A stoichiometric ratio (4:1) of water-to-Si-OR groups was utilized in all experiments to insure complete hydrolysis. No external catalyst was added to the system. Films of the hybrid materials were cast in the fashion as described for the parent material.

2.4. Thermal gravimetric analysis (TGA)

Silicate uptakes were determined using a TA Instruments TGA Q500 instrument. Samples were heated at 10 °C/min to 800 °C under a N_2 atmosphere. The percent char was measured as the percent mass remaining in the pan at 700 °C. Silicate uptakes are reported as the difference in percent char between the sSEBS and corresponding hybrid material sample.

2.5. Dynamic mechanical analysis

Plots of the dynamic storage modulus (E') and loss tangent, $\tan\delta = E''/E'$ (E'' = dynamic loss modulus) vs. temperature (T) were generated by a Seiko Instruments SDM5600 Viscoelasticity Analysis System using the DMS 210 Tension Module. Rectangular-shaped samples were tested at a frequency of 1 Hz over a temperature range from −120 to +350 °C with a heating rate of 2 °C/min. Glass transition temperatures (T_g) were taken as the temperature corresponding to appropriate peak maxima on $\tan\delta$ vs. T curves.

OOT temperatures were defined in terms of discontinuities in the form of sharp increases in shear storage modulus (G') vs. T curves for various frequencies. These plots were generated using a TA Instruments DMA 2980. Square samples with dimensions of 5×5 mm^2 with various thicknesses were subjected to an oscillatory shear with an amplitude of 15 μm. The temperature was increased using a temperature step program where the temperature is stepped in 10 °C increments and held at each temperature until a full cycle of oscillation is complete. In this way, the effective time scale of the experiment increases with decreasing frequency. Data points were taken at each temperature step.

2.6. Atomic force microscopy

AFM phase images were obtained using a Digital Instruments Dimension 3000 scanning probe microscope in the tapping mode. Samples for AFM analyses were prepared by cryo-microtoming at ~ −40 °C using a diamond knife and a film cross-section was embedded in epoxy in order to create a smooth surface. In tapping mode, a cantilever holding a responsive needle is rastered across the surface at a particular rate while the needle taps on the surface with a certain frequency. Phase images are created on the basis of the phase difference between the input and output responses of the cantilever. This provides a qualitative measure of the local viscoelastic properties in the vicinity of the needle. Due to the large difference in room temperature viscoelastic properties, between the hard and soft domains in SEBS, significant contrast can be generated in a phase image to allow for observation of the BCP morphology.

2.7. Small angle X-ray scattering (SAXS) analysis

SAXS data were collected at the Army Research Laboratories, Aberdeen, using a Bruker Hi-Star detector and Cu K_α radiation where $\lambda = 1.5418$ Å. X-rays were generated by a Rigaku Ultrax-18 rotating anode operating at 40 kV and 60 mA and filtered using a pyrolytic graphite monochromator. The camera length was 63.3 cm. Data were averaged azimuthally for analysis of scattered intensity, I, as a function of the magnitude of the scattering wave vector, q. The value of the scattering wave vector magnitude is given by $q = 4\pi\sin\theta/\lambda$ where 2θ is the scattering angle; the corresponding length scale, d, is given by $d = 2\pi/q$. Averaged data were inspected for Bragg peaks indicative of order and symmetry, and all data presented is in arbitrary intensity units.

3. Results and discussion

3.1. TGA

Representative TGA curves for hybrid materials for various percent silicate uptakes and the parent acid form sample are shown in Fig. 2. Actual percent uptakes are in good agreement with the targeted uptakes, based on pre-measured compositions, except for the sample at 20%. The final degradation of the sSEBS matrix occurs around 400 °C. It is a significant fact that, as opposed to other thermal properties, the degradation temperature is unaffected by silicate incorporation.

3.2. DMA analysis in tension mode

The influence of PS block sulfonation on E' vs. T behavior and thermal transitions of SEBS are seen in Fig. 3(a) and (b). There are two distinct glass transitions, one corresponding to the ethylene/butylene (EB) block domains at low temperatures, and the other to the sPS block domains at higher temperatures. The latter is seen to depend on degree of sulfonation. Between these two transitions, there is a rubbery plateau on the E' vs. T curves where the E' values increase with increasing degree of sulfonation. It is reasonable that sulfonation introduces strong hydrogen bonding interactions between different PS blocks so as to restrict chain mobility in these domains, which would account for the increase in plateau modulus. Another factor to consider is a change in morphology upon sulfonation that may cause an increased plateau modulus; this possibility will be addressed later.

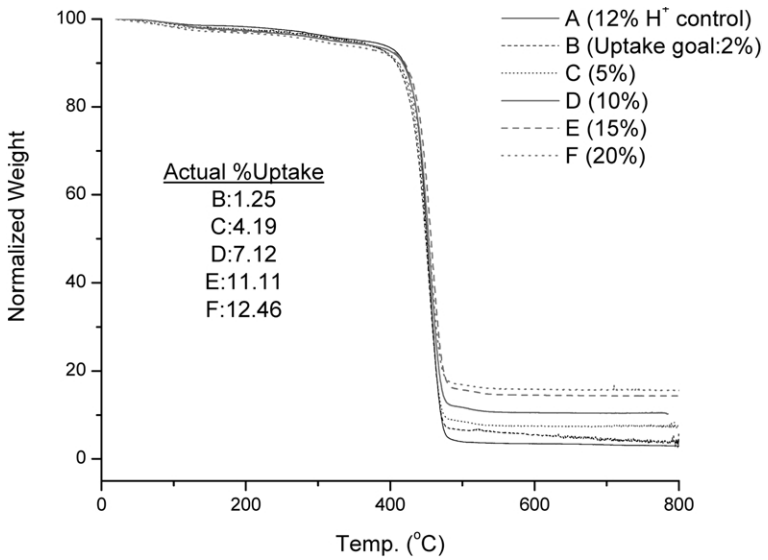

Fig. 2. TGA mass loss curves for various silicate percentages in sSEBS samples. All weights are normalized to 100%.

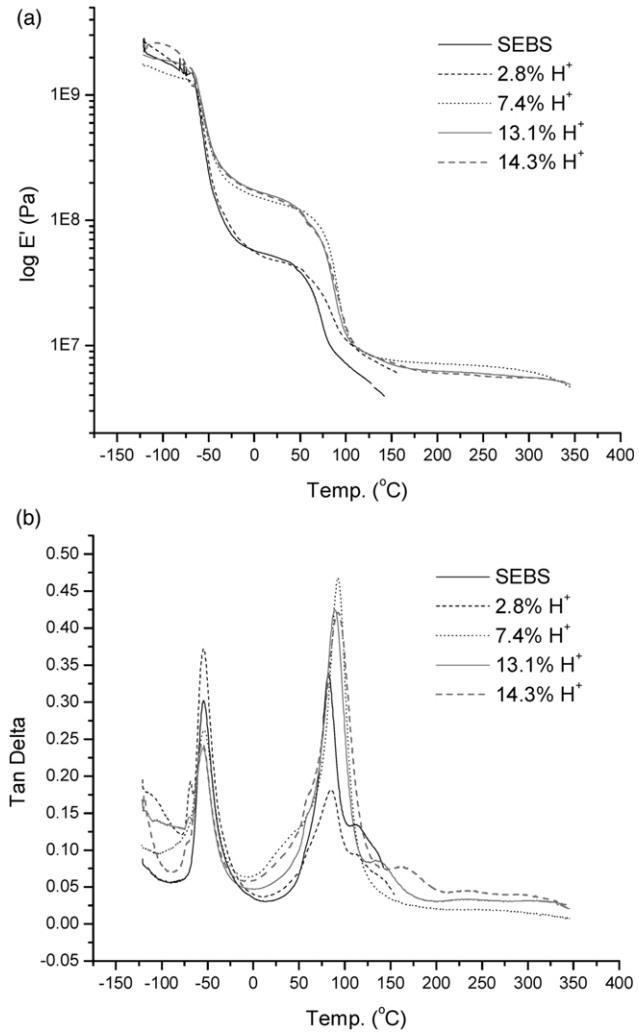

Fig. 3. (a) E' vs. T, and (b) tan δ vs. T curves for indicated sulfonic acid levels in the PS blocks of sSEBS.

In the terminal zone (i.e., at temperatures beyond the PS domain glass transition) of unmodified SEBS and 2.8% H^+SEBS, flow occurs in the sense of a precipitous drop in E', or loss of elasticity. However, for the samples that had greater degree of sulfonation, there is a second plateau that persists at least up to 350 °C. This phenomenon might also be due hydrogen bonding between SO_3H groups on different PS blocks even though the PS block segments are in a fluid state at these temperatures [40]. Assuming the validity of this view, flow cannot occur because the hydrogen bonding associations would not be disrupted before the temperature of thermal degradation of SEBS occurs.

Table 1 summarizes the effects of PS block sulfonation on the thermal transitions of SEBS. T_g for the EB block remains rather constant regardless of degree of sulfonation, but T_g for the PS block, in general, increases with increasing sulfonation. The sPS block T_g in the 7.4H^+ sample, however, is a departure from this trend, being slightly higher than that of the 13.1% H^+ sample and is equal to that of the 14.3H^+ sample. A possible explanation for this will be discussed in the light of other results discussed later.

A third transition that appears at temperatures beyond the PS block T_g is observed for the parent SEBS as well as for the sSEBS samples. The nature of this transition in the parent SEBS is not well understood although it has been suggested to be a domain disruption transition [41] prior to

Table 1
Thermal transitions for various degrees of SEBS sulfonation

Sample	EB block T_g (°C)	PS block T_g (°C)	High temperature transition (°C)
Parent SEBS	−54	82	114
2.8% H^+	−54	85	114
7.4% H^+	−54	92	–
13.3% H^+	−53	90	140
14.3% H^+	−56	92	166

the ODT. Another postulated mechanism consists of stress-induced alignment of the PS domains after there is sufficient chain mobility in this phase. It is difficult to make an unambiguous assignment for this transition because it occurs as the BCP enters a liquid-like condition in the instrument. In any case, it is believed that this high temperature transition in the parent SEBS is different than the high temperature transitions observed in the sSEBS materials.

The 7.4H^+ sample does not show the high temperature transition and the following facts, established for cross-linked sulfonated polystyrene [42], may be relevant. In this similar system, the SO_3H groups in thoroughly dried samples can associate by way of strong hydrogen bonds. However, these bonds can be easily disrupted and replaced by those with water molecules that also cause proton dissociation and two H_2O molecules per SO_3H group are sufficient for this to occur. This mechanism can be applied to the sPS-PEB-sPS system while accounting for additional complications. Despite the fact that the sulfonic acid groups are confined to the PS blocks, it would seem that hydrogen bonds in dried samples would occur more easily between SO_3H groups on different outer blocks than between groups on the same block. While all the samples were dried in these experiments, inordinate atmospheric moisture may have penetrated the 7.4H^+ sample in transference to the extent that strong SO_3H group associations were disrupted as described above. We have detected minimal water in some 'dried' samples using FTIR spectroscopy, although the exact amount is difficult to quantify. Water molecules are known to strongly attach to SO_3H groups so that they may first begin to desorb from the sample at temperatures above 100 °C. Since the high temperature transition is thought to be due to regions of these associations, it may not be present for this particular sample owing to unintended water.

Based on the studies of Weiss et al. [35], it might be considered that the third, high temperature transition in the sSEBS materials is due to the formation of a SO_3H-rich phase when the degree of sulfonation is sufficiently high. The materials in this work do not have $SO_3^-Na^+$ ion pairs in the PS blocks as in the materials of Weiss et al. However, there can be proton dissociation in the low pK_a sulfonic acid groups in the presence of water that give rise to strong electrostatic interactions between -$SO_3^-H_3^+O$ charged moieties during film formation. After sample drying, PS chain segments in the vicinity of associated acid groups, between which there are strong electrostatic, or at least hydrogen bonding interactions, will have restricted mobility in a manner similar to that as described by Eisenberg et al. in their multiplet-cluster model for ionomers [43]. While this qualitative model was based on random ionomers, the general concept of regions of restricted mobility that overlap, so as to form a distinct sub-phase within the PS domains that have their own glass transition, is reasonable. T_g for this PS block sub-phase would be greater than that for an unsulfonated PS phase and would increase with increasing degree of sulfonation. We have observed that this third transition is significantly influenced by time of annealing at 120 °C [44]. If the films are annealed for at least 3d, this transition disappears for lower, and broadens at higher sulfonation degrees. Assuming the existence of such a sub-PS domain morphology, the formation of SO_3H group aggregates that reduce PS block conformational entropy would be kinetically driven. Restructuring would take place as an equilibrium state is approached by the addition of thermal kinetic energy via annealing. Strong SO_3H associations would be disrupted, and, for lower acid levels, aggregates of these associations would no longer be of a size that is sufficient to constitute a separate phase. This would apply for the 7.4% H^+ sample, which may have a transitional degree of sulfonation where the regions of restricted mobility are minimally large enough to overlap so as to form clusters. Perhaps the annealing conditions were sufficient to disrupt marginally stable clusters such that the third transition is not observed. However, SO_3H groups in associations that exist before annealing would be dispersed by heating. It is stressed that the above concepts are in the realm of speculation and are offered as possible mechanisms for consideration.

Fig. 4 (a) and (b) show the effects of silicate

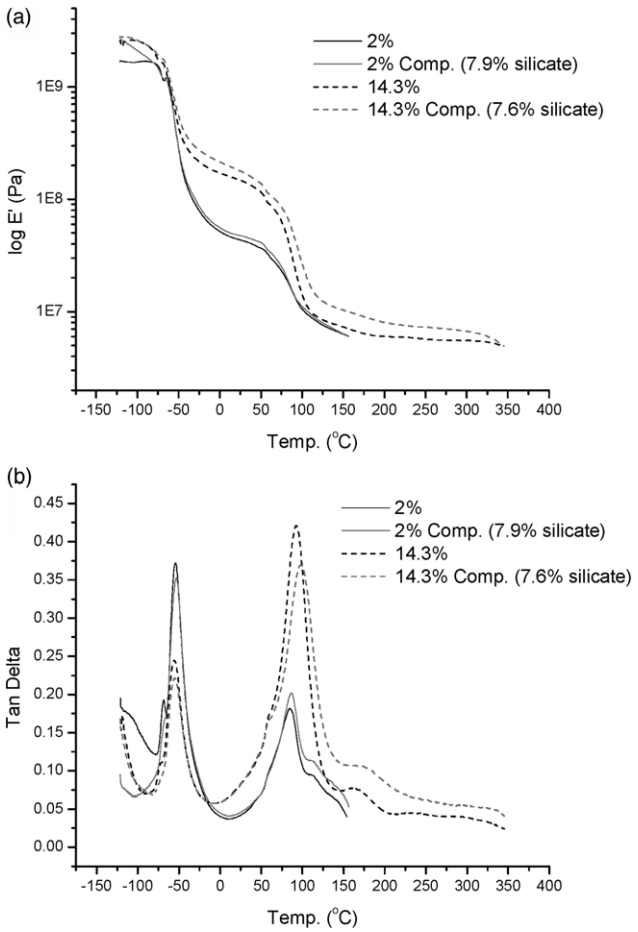

Fig. 4. (a) E' and (b) tan δ vs. T curves for two sSEBS samples and corresponding sSEBS/silicate composites.

incorporation on E' and tan δ vs. T behavior, respectively. Table 2 lists the temperatures of the transitions observed on these curves. While there is a significant difference between the curves for the two degrees of sulfonation, the plateau region on the E' curves is elevated only slightly when a given sSEBS sample is imparted a silicate phase. This might suggest that there are at best weak interactions between the continuous rubbery EB phase and silicate component in the sense of influencing the resistance to small dynamic mechanical deformation.

Silicate insertion essentially exerts no influence on the EB phase T_g for either percent sulfonation, although T_g(EB) does increase slightly when the degree of sulfonation increases. For the sPS phase T_g there is a discernible elevation for the 2.8% H^+ and significant elevation for the 14.3% H^+sSEBS with silicate incorporation. T_g(PS) for the 14.3% H^+/silicate sample is 11 °C greater than that of the 2.8% H^+/silicate sample. Also, the temperature of the third transition above the sPS T_g is elevated for the 14.3% H^+ relative to the 2.8% H^+ sample and this temperature for the silicate containing 14.3% H^+ sample is a significant 61 °C greater than that of the unfilled 2.8% H^+ sample.

This information is useful in assigning the location of the silicate component in the 2-phase sSEBS morphology. The fact that the sPS T_g increases while the EB T_g remains constant indicates that silicate quasi-networks essentially reside within the sPS domains rather than the EB domains.

At least for the samples listed in Table 2, it appears that sulfonation, rather than silicate structures affect chain mobility to some extent in the EB phase.

Thus, a template action in the sense of domain-targeted sol–gel reactions seems to be operative from the perspective of DMA. Since the sSEBS polymer morphology developed while the sol–gel reactions were taking place in the same solution during film formation, these heterogeneous materials can be said to be self-assembled, which is also verified by microscopic studies to be discussed.

Furthermore, the increase in temperature for the high temperature ($> T_g$(PS)) transition for the 14.3% H^+ sample with silicate incorporation also suggests that hydrolyzed TEOS monomers migrate to the sPS domains, and more specifically, to the sub-regions of sulfonic acid group aggregation.

At this time, the more specific question of whether the silicate component actually comes to reside in the sPS domains, or at interfaces, cannot be answered with certainty. The former would seem to the more reasonable within the context of a self-assembly process as well as the fact that the EB phase is not affected from the standpoint of chain mobility. If the growth would be at interfaces, some of the silicate branches that grow as the result of condensation reactions would have an opportunity to penetrate the EB phase from these locations. What is quite clear from the DMA experiments, in a general sense, is that the silicate component is essentially associated with the sPS phase.

Finally, it is important to note that efforts to incorporate a silicate phase in unsulfonated SEBS have been unsuccessful. This fact demonstrates the basic necessity of providing a polar environment in the PS phase that is compatible with hydrolyzed TEOS monomers so as to affect domain targeted sol–gel processes.

3.3. Order–order transition

Weiss et al. [33] reported an order–disorder transition (ODT) for this particular SEBS polymer that occurred at a temperature of ~240 °C based on their SAXS studies of temperature dependent morphology. These investigators monitored a scattering intensity peak with increasing temperature and the ODT was defined in terms of the temperature at which the magnitude of the peak diminished significantly. At this temperature, there is a loss of electron density contrast between two phases that was assumed to be due to hard/soft block endothermic mixing.

The dynamic mechanical investigations to be described here were initiated for the purpose of studying the dependence of this reported ODT on sulfonation and subsequent silicate incorporation. This high temperature process would be significant in relation to the thermal processing of these heterogeneous materials. DMA, in this case in shear rather than tensile deformation mode, was utilized to identify thermal transitions in the high temperature regime. At sufficiently low oscillatory frequencies, appropriate to the slow relaxation process associated with this transition, an ODT would, in principle, be characterized by a discontinuous decrease in the shear storage modulus, G', that is, loss in elasticity, as phase separation disappears. This, of course, is a phenomenological, rather than direct structural characterization of this transition.

The resultant G' vs. T data for unmodified SEBS at several frequencies are shown in Fig. 5. Rather than exhibiting a significant drop in G' at low frequencies, what is actually observed is a discontinuous increase in G' that develops with decreasing frequency. This material

Table 2
Thermal transition temperatures for sSEBS and sSEBS/silicate composites

Sample	EB Phase T_g (°C)	PS Phase T_g (°C)	High Temperature Transition (°C)
2.8% H^+	−54	85	114
2.8% Comp. (7.9% silicate)	−53	88	114
14.3% H^+	−56	92	166
14.3% Comp. (7.6% silicate)	−56	99	175

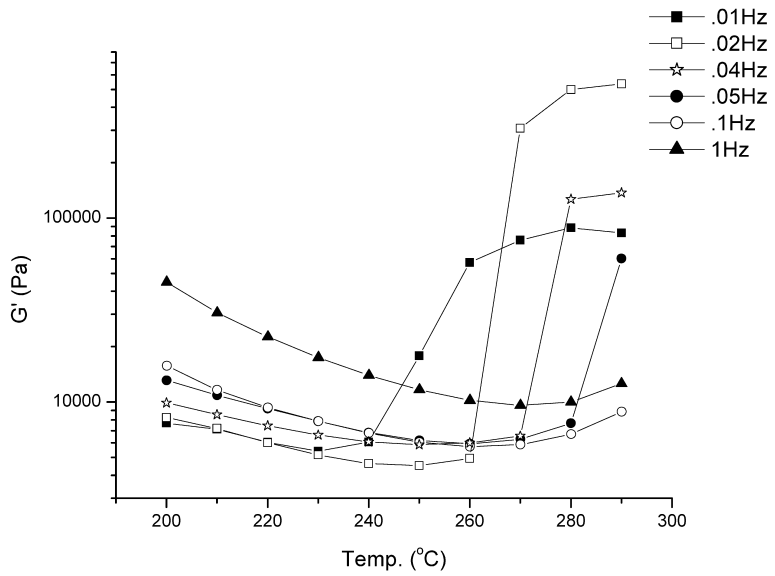

Fig. 5. Semi-log plot of G' vs. T for unmodified SEBS samples at various oscillation frequencies.

stiffening is more suggestive of a change in morphology rather than a disappearance in phase separation. While an ultimate gradual increase in G' with increasing T is seen on these curves at all frequencies, the upswing appears more abruptly, more akin to a transition, starting at 0.05 Hz and becomes more prominent for lower frequencies. The midpoint of the range of temperatures over which this transition takes place decreases with decreasing frequency. A decrease in frequency increases the time scale of the experiment such that the macromolecular rearrangements involved in a transition can be detected. Conversely, if the period of oscillation is decreased (higher frequency) macromolecular rearrangements involved in a transition must be activated by adding thermal kinetic energy, i.e., shifting to higher temperatures.

While others have observed order–order transitions to be independent of frequency below the critical frequency at which it first appears, the method used in these studies demonstrates the kinetic nature of this transition observed for these particular samples. As discussed in Section 2, the DMA method used in these studies involves a temperature step rather than a continuous temperature ramp. The temperature is held constant until a complete cycle of oscillation is applied. This, in effect, subjects the sample to increasingly slower heating rates with lowered frequencies, and, as the heating rate decreases, the transition shifts to lower temperatures and is more readily detected.

At 0.01 Hz, the OOT for SEBS is ~240 °C, which corresponds well to the temperature at which the scattering peak diminished in the SAXS experiments of Mani et al., and is 65 °C higher than the OOT observed by SAXS for a 12% H^+ sample [33]. Even at the low frequency of 0.01 Hz, no ODT was apparent in the SEBS sample up to 350 °C. The repeatable experiments were not conducted above 350 °C, which is approaching the degradation temperature.

Several researchers found the OOT in similar materials to be thermally reversible. Sakurai et al. [45] and Hajduk et al. [46] observed reversible transitions from HPC to BCC and from L to HPC morphologies, respectively, in diblock copolymers using SAXS and TEM analyses. Kim et al. found the OOT of polystyrene-*b*-polyisoprene-*b*-polystyrene to be reversible using DSC [13] and rheological methods [10]. However, we found no evidence of reversibility in SEBS using the rheological measurements as discussed below.

Fig. 6 is a semi-log plot of G' vs. T at 0.01 Hz, from data resulting from heating, subsequent cooling, and reheating unmodified SEBS over the indicated temperature ranges. What appears to be an OOT is obvious during heating to 300 °C, but no reverse transition is discernible when cooling the sample from 300 °C to 100 °C. The elastic component of the shear modulus that has accumulated up to the highest tested temperature does not reversibly decrease with decrease in temperature and in fact gradually increases. This result does not eliminate the possibility that this transition is reversible under other conditions because the kinetics of phase reorganization might in fact be too slow in these experiments to detect within the time frame of this experiment.

In this experiment, after the sample was cooled to 100 °C, it was annealed for 3 h at this temperature and then the temperature was increased back to 300 °C. After annealing for this time at 100 °C, there was only a slight drop in G' and during reheating no transition in the form of a step rise in G' occurred. Thus, the OOT, defined in this way, is irreversible, at least within the time frame of this particular experiment. Considering that annealing at 100 °C for 3 h does not impart sufficient chain mobility to induce a reverse transition, another experiment was conducted in which a sample had undergone a similar cycle that began at 150 °C rather than 100 °C. Upon cooling from 300 °C to 150 °C, the sample was annealed for 12 h at the latter

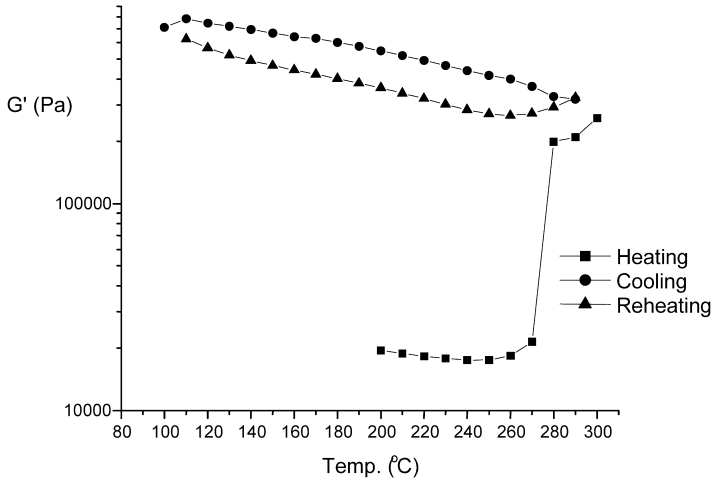

Fig. 6. G' vs. T for heating, subsequent cooling, and reheating unmodified SEBS. The sample was annealed for 3 h at 100 °C before reheating to 300 °C.

temperature and then reheated in the same fashion. The results, seen in Fig. 7, clearly do not show a reversible transition.

It may seem unreasonable that a transition from, say, a locked-in BCC to HPC morphology during the annealing step is much slower than a reverse transition because the BCC morphology is of higher energy for this PS composition. The fact that this is not the case implies that the transition mechanism is different for the forward (increasing T) than for the reverse (decreasing T) directions. It might be considered that a transitional state from, say BCC to HPC may require significantly higher activation energy than the transition from HPC to BCC. When considering the transition in both directions, this becomes more obvious. The transition from HPC to BCC is said to involve an intermediate morphology that has been described as undulated cylinders [17] where the cylinders become increasingly pinched until they finally break into spheres. This process does not involve complete morphological disruption. The reverse reaction would have to involve a fusion of spheres into cylinders. The energetic penalty associated with a morphological disruption would be too great (consider that the ODT must occur after 350 °C). Perhaps, instead of a transition from BCC to HPC upon cooling from above the OOT temperature, there is a change in the packing order of the spheres in a drive to minimize surface area, e.g., packed more densely so as to contact each other without coalescence. In any case, the situation is unclear and more investigations are required to uncover the actual mechanism of morphological re-ordering.

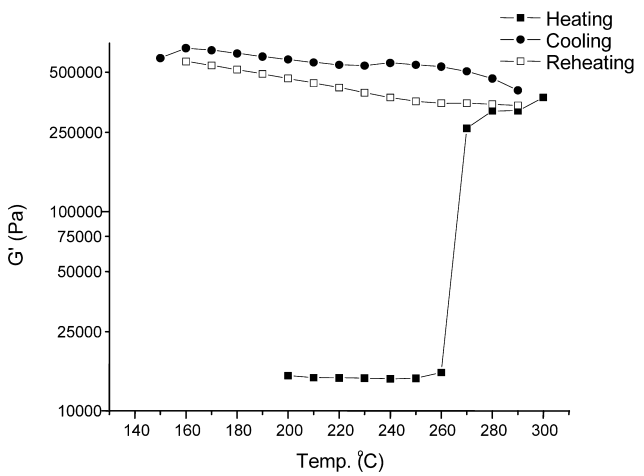

Fig. 7. G' vs. T for heating, subsequent cooling, and reheating unmodified SEBS. The sample was annealed for 12 h at 150 °C before reheating to 300 °C.

The influence of degree of sulfonation on the OOT is seen in Fig. 8. A significant increase in the OOT temperature of 20–25 °C occurs after only 2% sulfonation, although a maximum of 290 °C is reached at 7% sulfonation. This might be rationalized in terms of a decrease in PS block segmental mobility resulting from hydrogen bonding interactions between SO_3H groups. There must be sufficient mobility for PS cylinders to rearrange into spheres (—if, in fact, the transition is to BCC), and, as the number of these interactions increase, higher temperatures are needed to overcome the increased cohesion in the PS phase, thereby increasing the OOT temperature.

Sulfonation greatly increases the polarity of PS blocks relative to EB blocks, thereby increasing χ_{S-EB}. This would have the effect of inducing more distinct phase separation with smaller interphase thickness. During the macromolecular rearrangements occurring during an OOT some chains would necessarily diffuse across interphase regions. Decreased PS–EB block compatibility would make movement of PS blocks across interphases less favorable. An increase in χ_{PS-EB} also results in an increased thermodynamic opposition to an increase in interfacial area that would occur at an OOT.

In Fig. 8 there is another event in the form of a second, higher temperature step rise in G' for the 2 and 4.5% H^+ samples. This transition is more sensitive to sulfonation level, showing a 30 °C increase in temperature from 2 to 4.5%, which is in contrast with the first transition that only

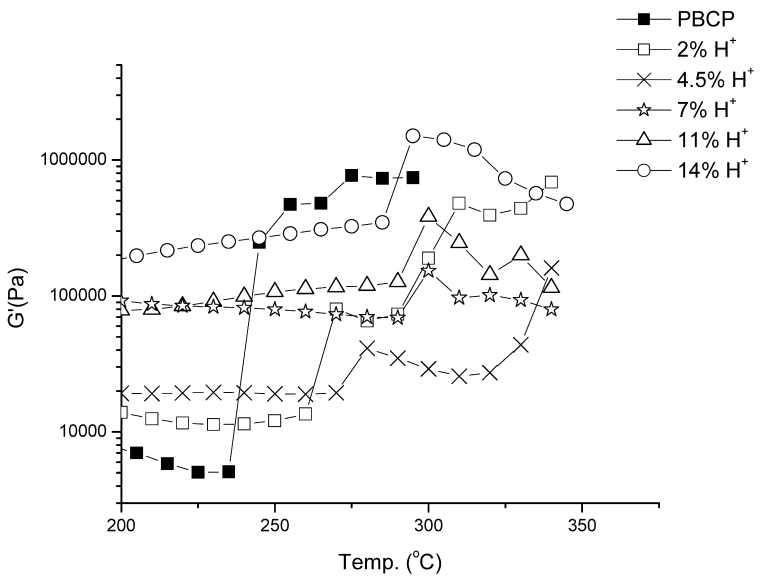

Fig. 8. Semi-log plot of G' vs. T at 0.01 Hz for the indicated degrees of sulfonation. PBCP = parent block copolymer.

showed a 10 °C increase. Perhaps a second order–order transition exists above 350 °C for higher H^+ levels that is due to a morphological change induced by sulfonation. It might be speculated that at 2% H^+ there is incomplete shifting between equilibrium mesophases such that the morphology is trapped in an intermediate state, and at 4.5% H^+ the mesophase shift may be more complete. As discussed later, the AFM results show a morphological transformation from the familiar equilibrium mesophases upon low sulfonation, and provide support for this idea.

In the simpler Surlyn® [47] or sulfonated EPDM (ethylene–propylene–diene monomer terpolymer) ionomers [48], ionic associations can be disrupted by heat, allowing the polymer to flow, and these associations can reform upon cooling. The sPS-EB-sPS systems described here are more complex owing to the fact that there is more than one phase, each being larger than the ionic multiplets in Surlyn® and in sulfonated EPDM, so that ionic aggregate disruption must be coupled to hard/soft block phase reordering. Also, there are no hard ions in the system. The simple fact that there is irreversibility in the unsulfonated samples indicates that the dynamics of SO_3H associations are not basic to understanding this phenomenon.

There might also be concern regarding thermal degradation of SO_3H groups and its possible influence on this transition. The following comments are based on the behavior of somewhat similar systems. Again, the simple but important fact is that the irreversible transition occurs in unmodified SEBS as well as in the sulfonated version, which eliminates a mechanism of sulfonic acid group degradation as a primary cause of this phenomenon, although this may influence the transition. The TGA curves show no distinct mass loss event at 300 °C that might be associated with large scale SO_3H group degradation as seen in other studies of systems involving sulfonated polystyrene. The gradual mass loss from the lowest temperature is usually associated with the evolution of residual solvent, including water. Gupta and Scherer investigated the degradation of radiation-grafted and sulfonated poly(tetrafluoroethylene-hexafluoropropylene)-*g*-polystyrene membranes using TGA, and by measuring the ion exchange capacity (IEC) of degraded samples [49]. They reported a degradation temperature of 310 °C that preceded PS chain degradation. However, their IEC determinations showed that sulfonic acid group loss initiates at just beyond 200 °C in this particular system. In a study of a very similar system as that of Gupta and Scherer, Nasef investigated the thermal stability of radiation grafted PTFE-*g*-polystyrene sulfonic acid materials [50]. TGA thermograms showed a weight loss step at ~300 °C that was attributed to the loss of sulfonic acid groups and the evolution of SO_2 also takes place at this temperature. IEC vs. temperature plots showed that the sulfonic acid groups are stable until 200 °C and have an initial desulfonation temperature of 250 °C for samples heated in an oven (as opposed to a TGA instrument). These results are in harmony with those of Gupta and Scherer [49] and both groups suggested that two SO_3H groups of adjacent chains react with each other to generate SO_2 and H_2O and this creates a chemical crosslink. These irreversible crosslinks would, of course cause irreversibility when the sample is cooled from the highest-tested temperature.

Fig. 9 shows the effect of silicate incorporation relative to that of different degrees of sulfonation. Silicate incorporation is seen to increase the OOT temperature for a given degree of sulfonation, but there is a more profound difference between the unfilled samples having different degrees of sulfonation. Assuming that the inorganic phase resides primarily within the sulfonated PS domains, the silicate quasi-network structures can be thought of as restricting PS block mobility. The fact that the OOT temperature increases markedly, especially in the case of the 2% H^+ samples, adds support to the idea that the sulfonated

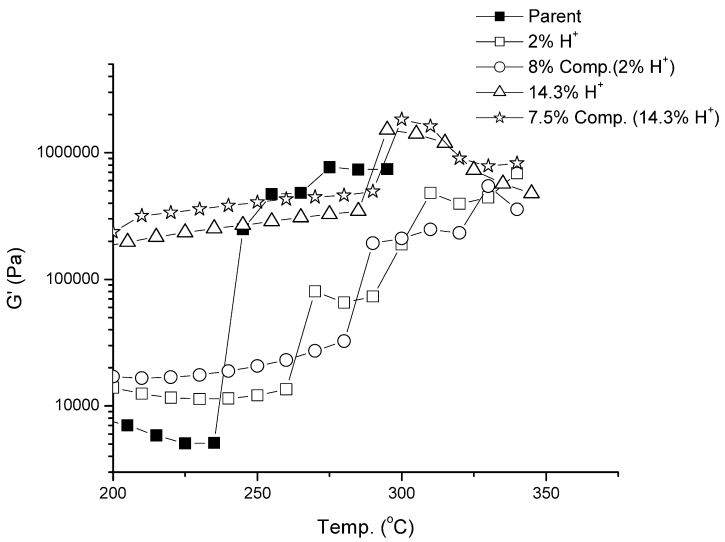

Fig. 9. G' vs. T at 0.01 Hz for two degrees of sulfonation and two corresponding silicate-containing composites.

PS domains provide an environment that is energetically compatible to the sol–gel reactants and silicate network formation. There may be a second, less intense transition in the 2% H^+ form composite at ~320 °C. Either the second transition has been shifted beyond 350 °C, or hybrid formation has again altered the morphology. The influence of silicate incorporation on morphology will be addressed in the following section. Table 3 summarizes the results from Figs. 8 and 9.

A more complete view of the effect of silicate uptake on the OOT of sSEBS is seen in Fig. 10. In this case, the 10% H^+ sSEBS control displays a broad transition that begins with an increase in G' at 280 °C and extends over a temperature range of ~30 °C. The sample containing 14% silicate shows a transition that also begins at 280 °C, but is much sharper and spans a temperature range of only 10 °C. The composites with 18 and 25% silicate uptake also have a transition that begins at 280 °C, although a sharp transition is not observed in these samples until 290 and 300 °C, respectively. For all three composites, not only is the transition sharper, but the increase in G' is around three times greater than that for the acid form control. In addition, all of the silicate-containing samples showed a sharp decrease in G' following the transition, whereas, the control sample maintained an elevated modulus up to 350 °C. The explanation for this remains unclear. A final observation from Fig. 10 is that the 18 and 25% composites had higher G' values prior to the transition, relative to the acid form, at these elevated temperatures.

Table 3
OOT temperatures for BCPs of various degrees of sulfonation and corresponding sBCP/silicate hybrids

Sample	OOT Temp. (°C)
PBCP	235
2% H^+	260
4.5% H^+	270
7% H^+	290
11% H^+	290
14% H^+	285
2% H^+ Comp. (8% silicate)	280
14% H^+ Comp. (7.5% silicate)	290

4. Morphology

4.1. AFM analysis

Tapping mode/phase images for an unmodified SEBS sample are shown in Fig. 11. At 30 mol% PS composition, HPC morphology is expected and confirmed by these images.

As mentioned, PS block sulfonation can disrupt the usual phase separated morphology, although this might not be expected at low sulfonation levels. However, in this case, there is a morphological transformation affected by low sulfonation such that the HPC mode is no longer present, as depicted in Fig. 12, where the morphology of 2% H^+SEBS does not fit into the usual scheme of PS phase geometry vs. copolymer composition. The new morphology appears worm-like with lamellar regions dispersed throughout, and might be termed ‘frustrated’ owing to the comparative disorder. The observation supports the concept of a second OOT, which would be the result of a transition from this ill-defined morphology to HPC for 2% H^+SEBS, as observed in the viscoelastic measurements. Fig. 13 is a TEM image of an 8% H^+sSEBS sample that also shows similar frustrated morphological features. The view of frustrated morphology is seen in both TEM and AFM images.

However, when the level of sulfonation reaches at least 12% a very distinct morphology exists that is neither frustrated HPC but clearly lamellar (L), as seen in Fig. 14; 12% sulfonation affects a complete mesophase transformation. This lamellar morphology has very well defined

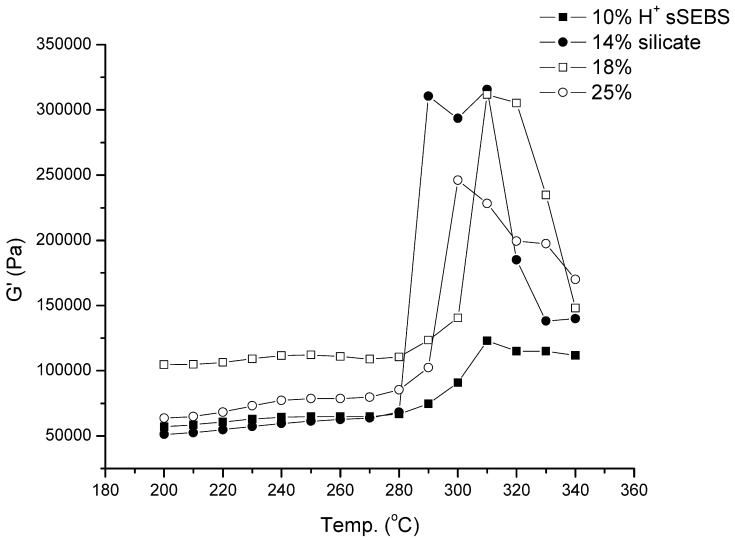

Fig. 10. G' vs. T at 0.01 Hz for (10% H^+ sSEBS)/silicate composites incorporating various percent silicate.

domains of sizes (i.e., the width of the white features in the micrograph), on the order of 20–30 nm. A tapping mode/phase image of a 14% H^+SEBS sample (not shown) shows essentially the same morphology as that in Fig. 14, which attests to experimental consistency. Fig. 15 is a TEM image, at higher resolution, of the same 14% H^+SEBS sample, which clearly shows the lamellar morphology that exists at this degree of sulfonation.

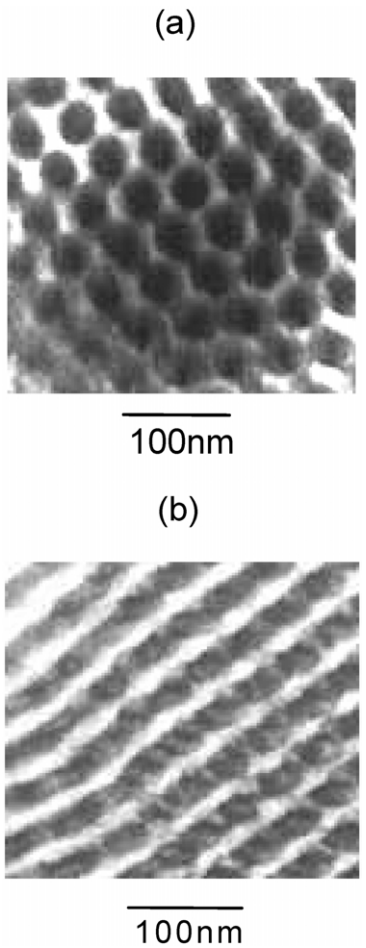

Fig. 11. TEM images of unmodified SEBS illustrating HPC morphology of PS cylinders that are (a) normal and (b) parallel to the plane of the image.

It is not believed that this lamellar morphology is of a non-equilibrium nature, say, being the result of improper annealing in the sense that sulfonation will raise the T_g and the viscosity of the PS blocks that would hinder structural development. The dynamic mechanical results indicate that T_g for the PS blocks never exceeds the annealing temperature and, moreover, annealing is conducted for considerable time to allow for structural relaxation.

After incorporation of 8% silicate into the 12% H^+SEBS structure, the lamellar morphology persists in striking fashion where domain thickness remains on the order of ~20–30 nm, as seen in Fig. 16. Thus, silicate phase insertion does not perturb the morphology of the sSEBS. Since the phase dimensions did not change, it can be concluded that the silicate phase dimensions are the result of a template process caused by the polymer under dynamic conditions. This also validates the concept that SEBS having higher degrees of sulfonation could exhibit a second OOT from HPC to BCC at temperatures above 350 °C.

4.2. Small angle X-ray scattering analysis

Figs. 17 and 18 show the averaged intensity, $I(q)$, as a function of scattering wave vector magnitude, q, for SEBS and sSEBS with 12% sulfonation, respectively. Both sets of data show multiple Bragg reflections that suggest ordered morphologies and the relative peak positions provide fingerprints of the specific morphology in each case [51]. For example, where the primary Bragg reflection is denoted q^*, a well-ordered lamellar morphology will exhibit Bragg reflections at integral multiples of q^*. On the other hand, HPC morphology should exhibit reflections at

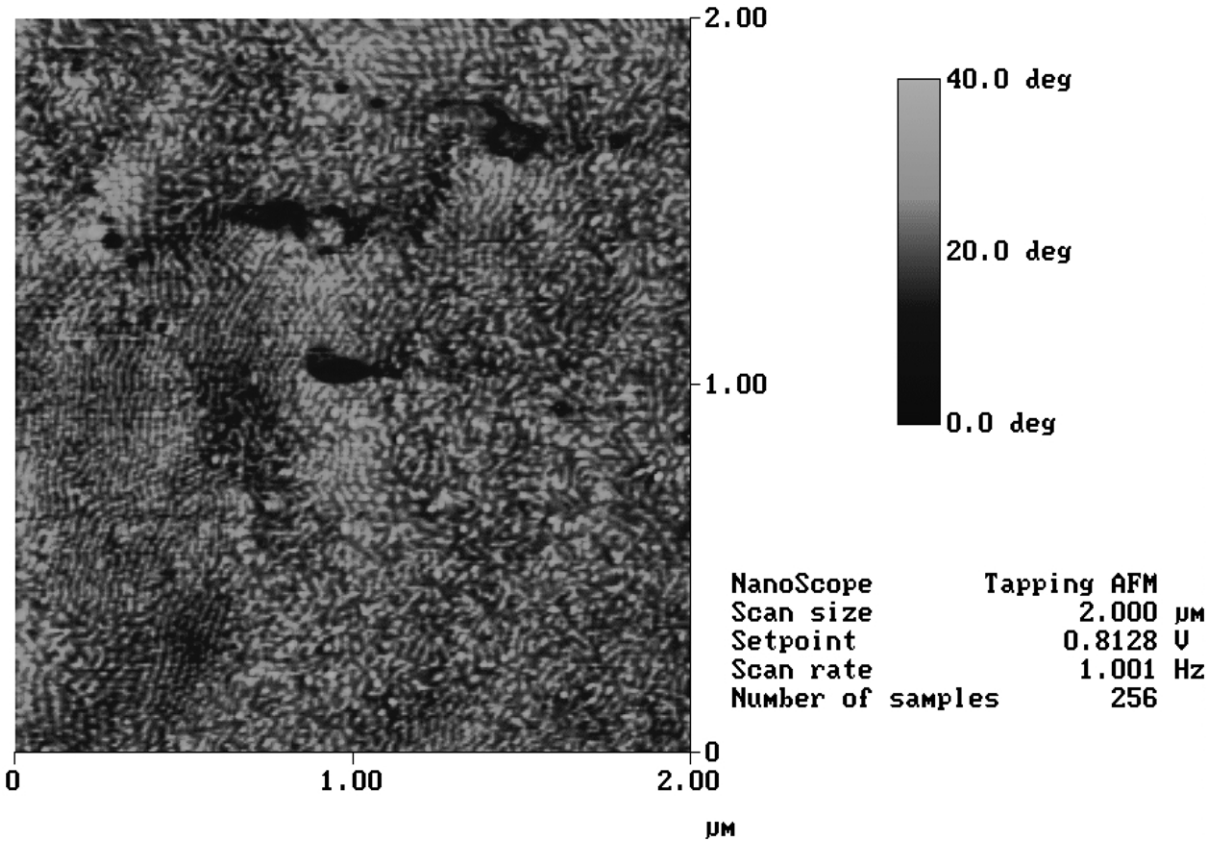

Fig. 12. Tapping mode/phase image of a 2% H^+ sample showing morphology over a broad field.

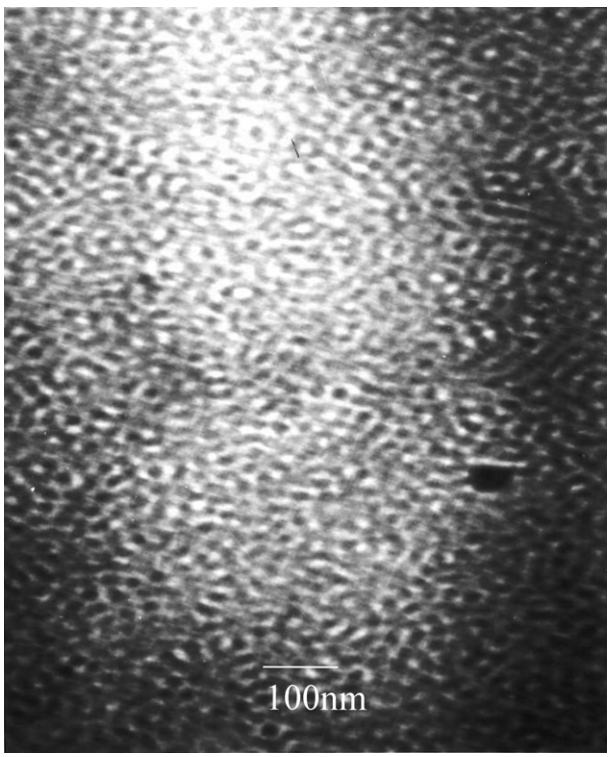

Fig. 13. TEM image of an 8% H^+ sSEBS sample showing a frustrated morphology.

$q^*, 3^{1/2}q^*, 2q^*, 7^{1/2}q^*, 3q^*$, etc. The critical reflection to observe for determination of spheres on a BCC lattice is the second Bragg reflection at $2^{1/2}q^*$.

In Fig. 17, Bragg reflections at $q^*, 3^{1/2}q^*$, and $7^{1/2}q^*$ are clearly visible, indicating HPC morphology, and the lack of a reflection at $2^{1/2}q^*$ eliminates spheres, in harmony with the TEM image for unmodified SEBS in Fig. 11. The absence of a reflection at $2q^*$ is not unusual, and may be due to the general weakness and breadth of the higher order reflections. The cylindrical periodicity is determined to be 26.2 nm.

The scattering data seen in Fig. 18 shows clearly multiple Bragg reflections arising from a well-ordered lamellar morphology for this sSEBS sample. The lamellar periodicity is determined to be 29.6 nm, which is in good agreement with the domain thickness determined by AFM.

The morphology shift induced by sulfonation remains to be explained. First, it might be considered that the addition of the steric volume of each SO_3H group to the PS blocks increases the volume fraction of the PS phase, f_{PS}. However, the particular volume increase affected in these cases would not be great enough to cause a switch in phase geometry unless the initial f_{PS} was already near the composition border between two mesophases. Second, it may be possible that the observed sSEBS morphology is simply of a non-equilibrium nature, being driven by restricted mobility of the PS blocks that slows the kinetics of film formation due to

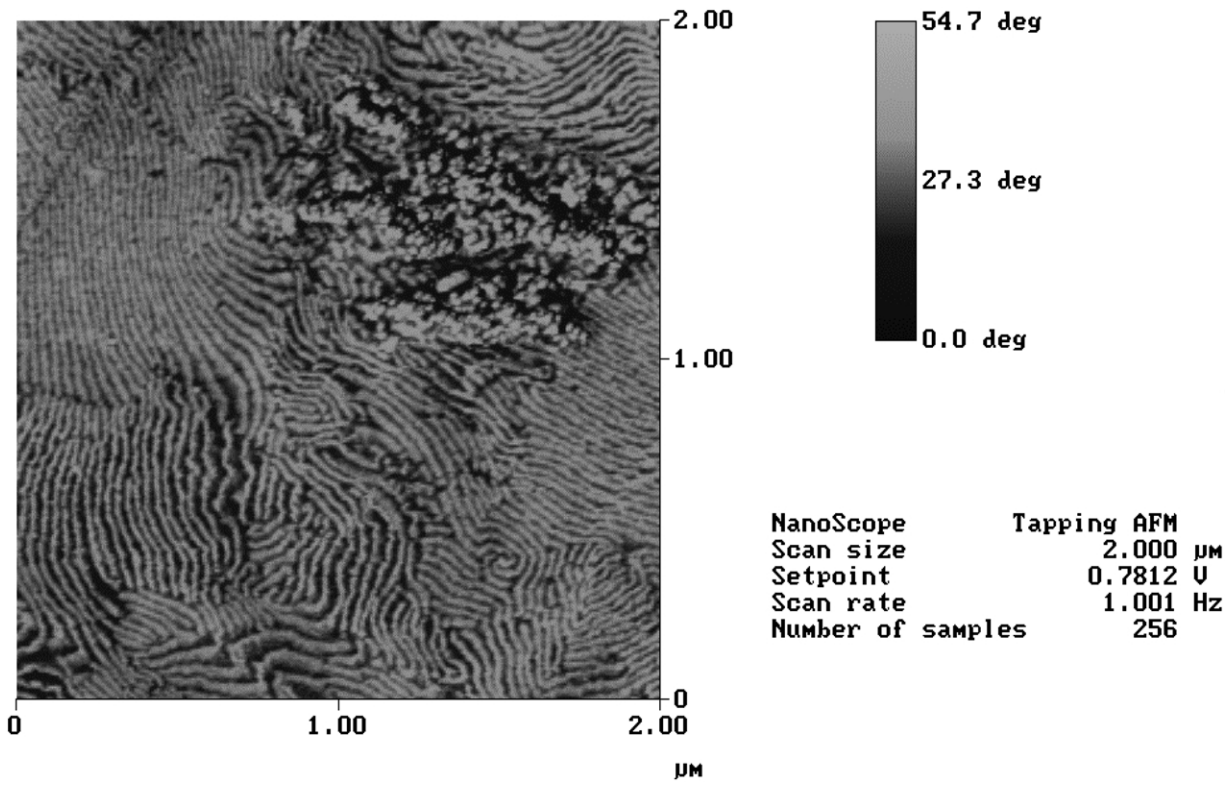

Fig. 14. Tapping mode/phase image of a 12% H^+ sample.

strong hydrogen-bonding interactions. However, the time-temperature annealing conditions employed during film formation would seem to be sufficient to attain a morphology that is at least close to equilibrium. Moreover, if restricted mobility were responsible for the disruption of the natural HPC morphology, we would not expect to see the well-defined morphologies as revealed by AFM.

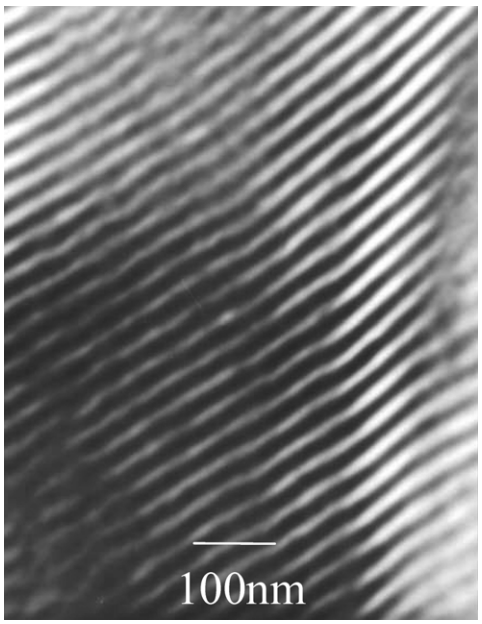

Fig. 15. TEM image of a 14% H^+ sSEBS sample showing lamellar morphology.

Perhaps these observations can be understood in thermodynamic terms by considering the quantity $\chi_{S-EB}N$ that, along with f_{PS}, determines phase separation. As mentioned previously, χ_{S-EB} increases with PS block sulfonation due to the increased polarity contrast between the two block phases. This also increases interfacial surface tension, which would affect a shift in morphology in the drive to minimize the interfacial surface area and reduce the surface tension. And so, it might be that the morphology observed for 2% H^+SEBS is an intermediate morphology with increased temperature instability. Sulfonation may also result in an effective increase in N in the form of hydrogen bonding between different chains.

5. Conclusions

Sulfonation of a SEBS triblock copolymer resulted in an increase in the dynamic plateau storage modulus as well as the formation of a new plateau at temperatures above the PS phase T_g. This material stiffening is tentatively attributed to hydrogen bonding interactions between sulfonic acid groups, in the hard block regions, that hinder block segmental mobility. Sulfonation does not affect the EB block phase T_g but increases the PS block phase T_g, which is likewise viewed in terms of hydrogen bonding interactions. Sulfonation causes a third, high temperature transition and it is speculated that this is due to the disruption of a SO_3H-rich PS sub-phase that is sensitive to annealing.

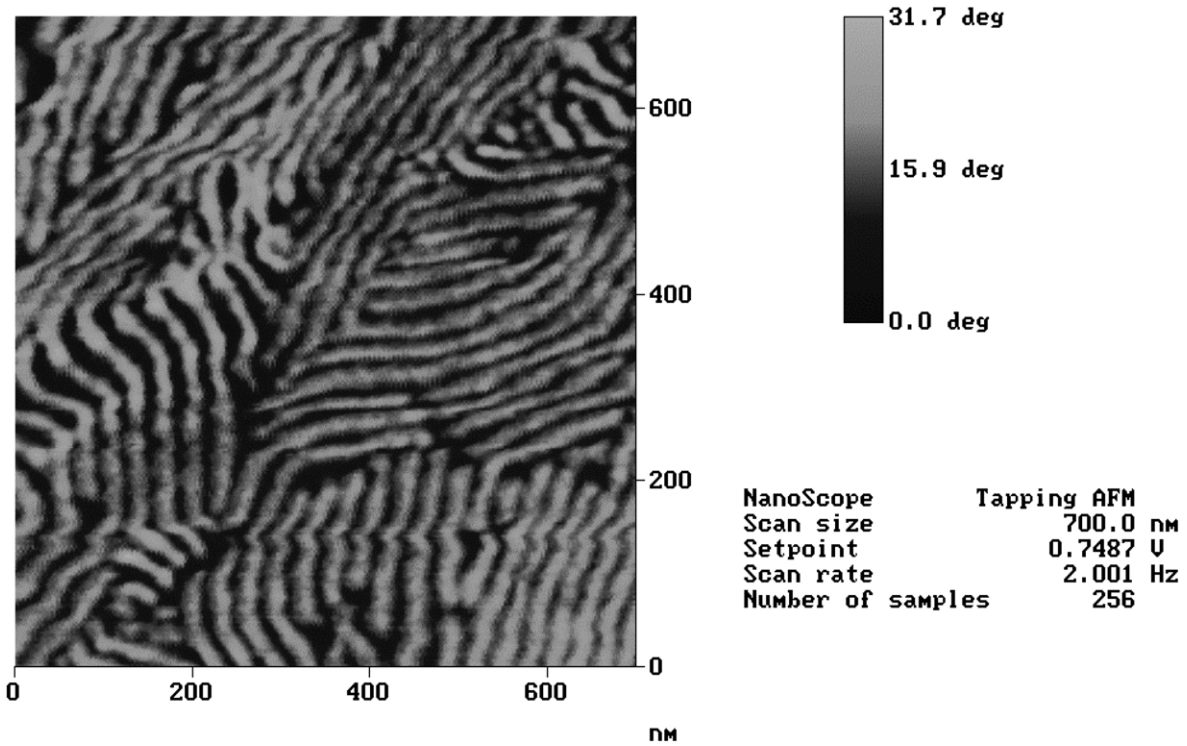

Fig. 16. Tapping mode/phase image of a 12% H^+ SEBS sample containing 8% silicate.

The rubbery E' plateau only elevates slightly when sulfonated SEBS is imparted a silicate phase via a sol–gel process for TEOS, which suggests only weak interactions between the continuous rubbery EB phase and the silicate component. The fact that the PS T_g increases while the EB T_g remains constant with silicate insertion indicates that the silicate quasi-networks essentially reside within the sPS domains rather than in the hydrogenated EB domains. Owing to the fact that the sSEBS polymer morphology evolved concurrent with the inorganic sol–gel process during film formation, these organic–inorganic hybrids are self-assembled materials.

DMA in shear mode showed that unmodified SEBS exhibits an irreversible OOT, characterized by a discontinuous increase in G', that develops with decreasing frequency, at ~240 °C. No ODT was observed up to 350 °C. Sulfonation caused an increase in the OOT temperature to ~290 °C, which is attributed to decreased PS–EB block compatibility and the addition of strong

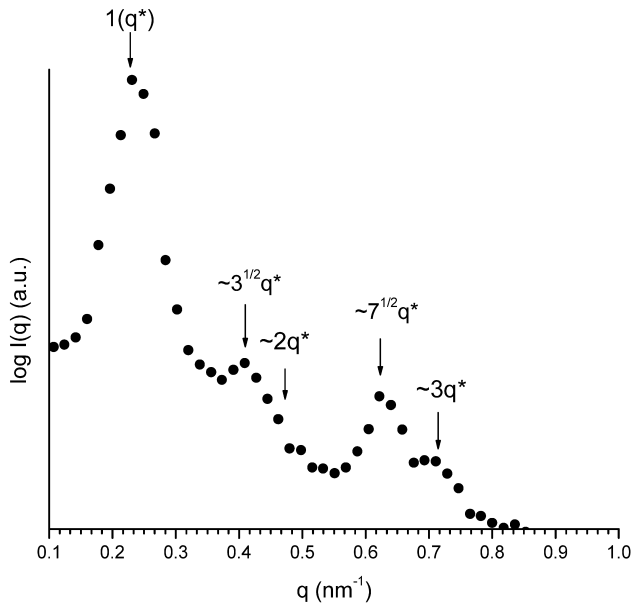

Fig. 17. SAXS profile for unmodified SEBS. The vertical axis is in arbitrary units (a.u.).

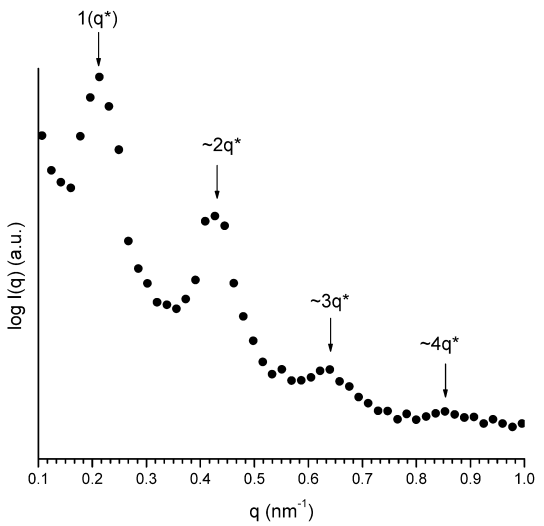

Fig. 18. SAXS profile for 12% H^+SEBS. The vertical axis is in arbitrary units (a.u.).

interactions between different sulfonated PS blocks. Sulfonation affected another, higher temperature transition at lower sulfonation degrees, consisting of a step rise in G' and this transition is more sensitive to sulfonation.

Silicate incorporation further increased the OOT temperature and this was rationalized in terms of mobility restrictions on chains imparted by invasive silicate nanostructures.

AFM, TEM and SAXS analyses confirmed that sulfonation causes a morphology shift from HPC to a frustrated morphology with worm-like features and lamellar regions at 2% sulfonation, while an increase in sulfonation to 12% generates a well-defined lamellar morphology. This can be rationalized in terms of chain mobility restrictions due to hydrogen bonding and an increase in χ_{PS-EB} and consequent higher interfacial surface tension.

After incorporation of 8% silicate in the 12% sulfonated sample, lamellar morphology persists and domain dimensions are undisturbed so that is concluded that there is a sol–gel template process caused by the polymer, and that these are indeed self-assembled materials.

Finally, thermogravimetric analysis revealed that the temperature of thermal degradation is unaffected by silicate incorporation.

Acknowledgements

The authors gratefully acknowledge the U.S. Army Research Office (DAAD19-01-0498) for their financial support and Kraton® LLC for the donation of the Kraton® G1652 material.

References

[1] Mauritz KA, Storey RF, Mountz DA, Reuschle DA. Polymer 2002;43:4315.
[2] Mauritz KA, Storey RF, Reuschle DA, Beck Tan N. Polymer 2002;43:5949.
[3] Hench LL, Ulrich DR, editors. Ultra-structure processing of ceramics, glasses, and composites. New York: Wiley; 1984.
[4] Blackwell RI, Mauritz KA. Am Chem Soc Div Polym Chem Prepr 2002;43(2):1341.
[5] Blackwell RI, Mauritz KA. Am Chem Soc Div Polym Chem 2003;44(1):1128.
[6] Blackwell RI, Mauritz KA. Am Chem Soc Div Polym Chem 2003;44(1):1132.
[7] Holden G, Legge NR, Quirk R, Schroeder HE. Thermoplastic elastomers. New York: Hanser; 1996.
[8] Thomas EL, Alward DB, Kinning DJ, Martin DC, Handlin DL, Fetters L. Macromolecules 1986;19:2197.
[9] Liebler L. Macromolecules 1980;13:1602.
[10] Rosedale JH, Bates FS. Macromolecules 1990;23:2329.
[11] Bates FS, Fredrickson GH. Annu Rev Phys Chem 1990;41:525.
[12] Chung CI, Lin MI. J Polym Sci, Polym Phys 1978;16:545.
[13] Bates FS. Macromolecules 1984;17:2607.
[14] Han CD, Kim J, Kim JK. Macromolecules 1989;22:383.
[15] Rosedale JH, Bates FS. Macromolecules 1990;23:2329.
[16] Forster S, Khandpur AK, Zhao J, Bates FS, Hamley IW, Ryan AJ, Bras W. Macromolecules 1994;27:6922.
[17] Han CD, Baek DM, Kim JK, Ogawa T, Sakamoto N, Hashimoto T. Macromolecules 1995;28:5043.
[18] Kim JK, Lee HH, Ree M, Lee K, Park Y. Maromol Chem Phys 1998;199:641.
[19] Modi MA, Krishnamoorti R, Tse MF, Wang H-C. Macromolecules 1999;32:4088.
[20] Owens JN, Gancarz IS, Koberstein JT, Russell TP. Macromolecules 1989;22:3380.
[21] Kim JK, Lee HH, Gu Q-J, Chang T, Jeong YH. Macromolecules 1998;31:4045.
[22] Roe R-J, Fishkis M, Chang JC. Macromolecules 1981;14:1091.
[23] Winey KI, Gobran DA, Xu Z, Fetters LJ, Thomas EL. Macromolecules 1994;27:2392.
[24] Sakamoto N, Hashimoto T. Macromolecules 1995;28:6825.
[25] Sakurai S, Umeda H, Taie K, Nomura S. J Chem Phys 1996;105(19):8902.
[26] Sakamoto N, Hashimoto T, Han CD, Kim D, Vaidya NY. Macromolecules 1997;30:1621.
[27] Kim JK, Lee HH, Sakurai S, Aida S, Masamoto J, Nomura S, Kitagawa Y, Suda Y. Macromolecules 1999;32:6706.
[28] Bates FS, Rosedale JH, Fredrickson GH. J Chem Phys 1990;92(10):6255.
[29] Jian T, Anastasiadis SH, Fytas G, Adachi K, Kotaka T. Macromolecules 1993;26:4706.
[30] Stepanek P, Lodge TP. Macromolecules 1996;29:1244.
[31] Reuschle DA, Mountz DA, Mauritz KA, Brister LB, Storey RF, Beck Tan N. Am Chem Soc Div, Polym Chem Prepr 1999;40(2):713.
[32] Mountz DA, Beck Tan N, Storey RF, Mauritz KA. Am Chem Soc Div, Polym Chem Prepr 2000;41(1):273.
[33] Mani S, Weiss RA, Williams CE, Hahan SF. Macromolecules 1999;32:3663.
[34] Lu X, Steckle Jr WP, Weiss RA. Macromolecules 1993;26:6525.
[35] Lu X, Steckle Jr WP, Hsiao B, Weiss RA. Macromolecules 1995;28:2831.
[36] Chen W, Feng H, Ye C. Polym J 1997;29(2):992.
[37] Huang ZH, Dong JH, Qiu KY, Wei. J Appl Polym Sci 1997;66:853.
[38] Ikeda Y, Tanaka A, Kohjiya S. J Mater Chem 1997;7(8):1497.
[39] Weiss RA, Sen A, Willis CA, Pottick LA. Polymer 1991;32:1867.
[40] Weiss RA, Sen A, Willis CA, Pottick LA. Polymer 1991;32:2785.
[41] Tse MF. J Adhes Sci Technol 1989;3(7):551.
[42] Zundel G. Hydration and intermolecular interaction: infrared investigations of polyelectrolyte membranes. New York: Academic Press; 1969.
[43] Eisenberg A, Hird B, Moore RB. Macromolecules 1990;23:4098.
[44] Blackwell RI, Mauritz KA. In preparation.
[45] Sakurai S, Kawada H, Hashimoto T, Fetters LJ. Macromolecules 1993;26:5796.
[46] Hajduk DA, Gruner SM, Rangarajan P, Register RA, Fetters LJ, Honeker C, Albalak RJ, Thomas EL. Macromolecules 1994;27:490.
[47] Longworth R, Nagel H. In: Tant MR, Mauritz KA, Wilkes GL, editors. Ionomers: synthesis, structure, properties and applications. London: Blackie Academic and Professional; 1997. p. 365.
[48] Makowski HS, Lundberg RD, Westerman L, Bock J. In: Eisenberg A, editor. Ions in polymers. Advances Chemistry Ser, 187. Washington, DC: American Chemical Society; 1980. p. 3.
[49] Gupta B, Scherer GG. J Appl Polym Sci 1993;50:2129.
[50] Nasef MM. Polym Degrad Stab 2000;68:231.
[51] Cullity BD. Elements of X-ray diffraction, 2nd ed. Reading: Addison-Wesley; 1978.